An Experimental Study on Lift Force Generation Resulting from Spanwise Flow in Flapping Wings

Young Sun Hong*

Korea Air Force Headquarter, KyeRyong, ChungNam

Abstract

Using a combination of force transducer measurement to quantify net lift force, high frame rate camera to quantify and subtract inertial contributions, and Digital Particle Image Velocimetry (DPIV) to calculate aerodynamic contributions in the spanwise plane, the contribution of spanwise flow to the generation of lift force in wings undergoing a pure flapping motion in hover is shown as a function of flapping angle throughout the flapping cycle. These experiments were repeated at various flapping frequencies and for various wing planform sizes for flat plate and spanwise cambered wings. Despite the previous identification of the importance of spanwise fluid structures in the generation of lift force in flapping wings throughout the existing body of literature, the *direct* contribution of spanwise flow to lift force generated has not previously been quantified. Therefore, in the same manner as commonly applied to investigate the chordwise lift distribution across an airfoil in flapping wings, spanwise flow due to bulk flow and rotational fluid dynamic mechanisms will be investigated to validate the existence of a direct component of the lift force originating from the flapping motion in the spanwise plane instead.

Key Word : Flapping Wings, Spanwise Flow, DPIV

Nomenclature

A	= axial force
a_T	= tangential acceleration
D	= drag
F_y	= force of the flapping wing in the y direction
L	= lift
N	= normal force
P_u, P_l	= pressure over the top surface of the wing and over the bottome surface of the wing.
R	= resultant force
V_T	= tangential velocity
$\vec{V}_{XYZ}$, $\vec{V}_{ryz}$	= velocity with respect to the inertial frame(XYZ) and reference frame(xyz)
$\vec{V}_{rf}$	= velocity of the control volume reference frame
α	= angular acceleration
ω	= angular velocity

* Major, Korea Air Force Headquarter
  E-mail : young_sun_hong@yahoo.com

ω_z = vorticity vector in two dimensional flow

θ = angle of the flapping wing along the flap arc

$\tau_u, \tau_l,$ = shear stress over the top surface of the wing and over the bottom surface of the wing.

Ⅰ. Introduction

For flapping wings, several mechanisms unique to the flapping motion produce much stronger spanwise flow than that observed in fixed wings. This spanwise flow is often associated with the Leading Edge Vortex (LEV) as axial flow in the core of the vortex[1,2]. This flow characteristic has been largely ignored with the exception of its suspected contribution to the stabilization of the leading edge vortex. Spanwise flow can be defined as flow that travels along the span of the wing from the root to the tip, more or less parallel to the leading edge. It can also be defined as any flow in spanwise plane. Spanwise flow is generally regarded as the one of disadvantages of fixed wings, because of the related induced drag. However, spanwise flow has been identified as one of the main characteristics of the aerodynamics of flapping wings. Even though the flowfield resulting from the flapping motion is thought to be dominated by flow in the spanwise direction when compared to chordwise direction, how spanwise flow affects the generation of lift force in insect and bird wings has yet to be quantified. Therefore, as lift is generally explained with chordwise or streamwise flow in fixed and flapping wing aerodynamics, spanwise flow effects can be used to explain, at least in part, how insects and some birds produce lift. Even if flat plate wings are flapped with zero chordwise pitch angle of attack and no relative wind, they have been shown to generate lift forces (positive and negative depending on the sense of the stroke assuming no feathering) due only to the flapping motion. It follows that spanwise flow in flapping wings can potentially be responsible for at the least, some contribution to lift force generation in insect and bird flight.

Ⅱ. Spanwise Flow and the Wingtip Vortex Effect

A. Fixed Wing

There is a component of flow in the spanwise direction over the finite wing in steady, level flight. The very nature of lift generation comes from the existence of higher pressure on the bottom surface and lower pressure on the top surface. A spanwise component of flow from the tip toward the wing root causes the streamlines over the top surface to bend toward the root and over the bottom surface to bend toward the tip. The high pressure air under the wing has a natural tendency to flow around the wing tip (Fig. 1).
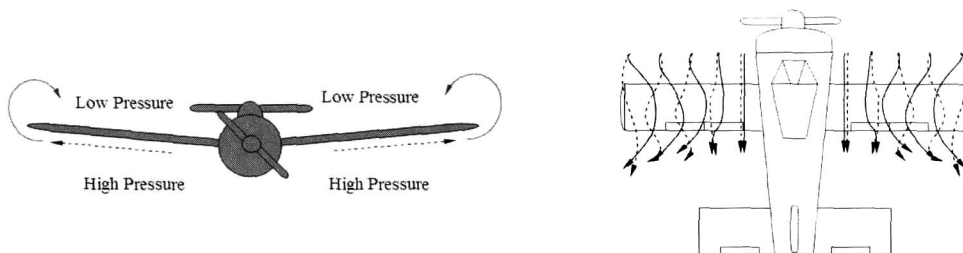

(a) Higher pressure air on the wing lower surface flows around the wingtip to the upper surface.

(b) Spanwise flow on a finite wing: the solid lines represent the upper surface; the dashed line is for the lower surface.

Fig. 1. Spanwise flow

More pronounced spanwise flow effects can be seen in wings with sweep. However, spanwise flow is generally regarded as the one of disadvantages of swept wings, because of the related induced drag. There is an increase in the lift near the tip of a swept back wing and a decrease in lift near the root, thus a swept back wing tends to have extra lift at the wing tips. One of the extreme examples of these swept wing effects is the delta wing. Delta wings are tremendously effective at low speeds and unsteady flows (Taylor[3]). Their leading edge vortices induce a field of low pressure on the suction side of the wing. However, for the case of the swept back or delta wing, research has, for the most part, focused on the disadvantages of spanwise flow and vortex effects on lift. Some research (Batchelor[4], Anderson and Lawton[5], Chow and Zillac[6] specifically investigates the proportional relationship between the axial flow velocity of the wingtip vortex core and circulation, and its relationship to the angle of attack and hence lift coefficient. Anderson and Lawton[5] showed the core axial velocity variation is a function of angle of attack, thus demonstrating that the vortex strength is proportional to the lift force. Khorrami[7] also mentioned that the vortex shows extremely low pressures in its core and the lower the core pressure drops, the higher the vortex rotational velocities become. Lian and Shyy[8] validated that wingtip vortices play an important role in low aspect ratio wing lift and that these vortices also reduce the effective angle of attack while bringing low pressure regions that provide additional lift. Despite the wealth of research performed relating lift to wingtip vortex circulation and behavior in traditional fixed wings for almost exclusively high Reynolds number aerodynamics, there has been no research to extend these fixed wing results to quantify the direct contribution of the wingtip vortex to the lift force in flapping wings.

B. Flapping Wings

As previously stated, spanwise flow has been identified in the form of axial flow within the leading edge vortex in flapping wings[1,2] and flow in the spanwise direction can be more dominant than flow in the chordwise direction depending on the forward velocity and rotational motion. Fig. 2 demonstrates that the span of the wings of over 1000 birds and insects taken from Greenwalt[9] correlate rather well with flapping frequency and reasonably well with body mass. These relationships could potentially be purely coincidental, however, there is also a good chance they could be indicative of the relative importance of the spanwise direction in the aerodynamics of birds and insects. There are no similar correlations for the chord lengths or wing areas of birds and insects as can be seen in Azuma[10].
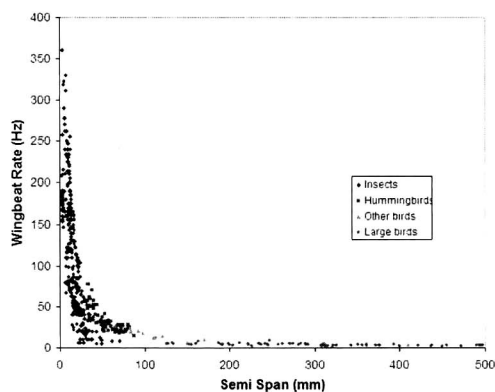
(a) Wing beat frequency versus wing semi-span of various insects and birds
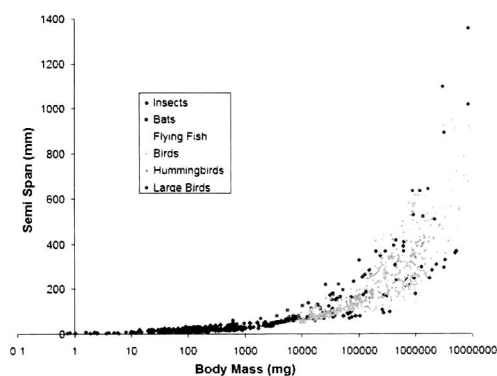
(b) Wing semi span versus body mass of various animals including insects, bats, birds

Fig. 2. Correlation between wingbeat frequency, wing semi-span and total animal mass show that span could be a dimension of interest[11]

Birch[12] validated that the rate of change in spanwise circulation with respect to the span is equal and opposite to the rate of change in chordwise circulation with respect to span. He also stated that a large percentage of the lift (~70%) experienced by the wing is due to the spanwise circulation. Therefore, analyzing the lift force due to flapping without the dominant rotational motion using the spanwise plane may be more reasonable than using the chordwise plane as these vortices must terminate somehow in hover. However, no literature was identified that explained lift force generation using spanwise flow and wingtip vortex effects in flapping wings.

III. Experimental Approach

A flat plate wing with zero degrees chordwise pitch angle of attack cannot produce lift using conventional chordwise aerodynamics alone. However, in hover, using asymmetric flapping mechanism with no forward relative velocity and zero degrees angle of attack, flapping flat plate wings produce lift. Therefore, the spanwise plane is proposed as another plane of potential interest in flapping wings without forward relative air speed. Under this assumption chordwise flow alone cannot account for the entire lift force necessary to lift birds and insects. In the experiments performed for this paper, the flapping motion is considered pure (downstroke and upstroke). No changes in chordwise pitch angle are made.

The experimental procedure consisted of three primary components:

1) Measurement of the Lift Force Generated by the Flapping Mechanism through Force Transducer Measurement – The total lift force was measured using an Interface SSM-AJ-250 "S" Beam force transducer with a maximum nonrepeatability of less than 0.02% and a maximum creep in 20 minutes of less than 0.025%. Total lift force was saved with 1000 data set per second during flapping cycles and averaged across 50 flapping cycles.

2) Determination of the Inertial Force Contribution to the Total Lift Force Generated through the use of a High Speed Camera – The net aerodynamic force is determined from this measured total force by subtracting the experimentally determined inertial and added mass contribution. A high frame rate camera (FASTCAM – Ultima ADX-1000 frame/sec) was used to permit experimental determination of the inertial forces of the flapping mechanism.

3) Measurement of the variation and distribution of spanwise planar flow velocity throughout the downstroke and upstroke to determine the magnitude of the lift force related to spanwise flow using the Digital Particle Image Velocimetry (DPIV) technique.

The details of each phase within the experimental procedure are provided in Section V, however, the force distribution along the span and the force variation during the flapping cycle are estimated using a control volume approach and pressure and shear force distribution based on the velocity data obtained from the results of the DPIV.

Fig. 3 shows the set up for the DPIV experiment. The Megaplus ES 1.0 cameras support the "frame straddling" mode of image acquisition required for short inter frame times required for PIV image acquisition. The camera synchronization with the frame grabber (EPIX) and laser firing (Spectra Physics, double pulsed 300 mJ/pulse 10 pulse/second Nd:YAg) is controlled via the strobe signal of the camera. The delay generator (DG 535) can be used to trigger the PIV laser flashlamps and Q Switches. The pulse that sends a signal starts all of the timing events, and is in phase with the laser repetition rate. The trigger pulse from the flapping motion is used to trigger the frame grabber. To trigger the pulse using the flapping motion, an emitter and detector are installed aligned with the peak of the flapping motion. If the flapping wings interrupt the emitting beam from emitter to detector, the detector produces a regular signal. The laser beam was split through a cylindrical lens to generate the light

sheet. The light scattered by the smoke particles (0.2 2 μm) is recorded on a 1k x 1k 8 bit progressive scan CCD camera using 25mm Cosmicar C mount lens. The PIV images were taken at numerous locations along the span, and at numerous chordwise stations for each spanwise location. DPIV (ISSI) was used for post processing using a 64 pixel correlation size of and a 50% image overlap.
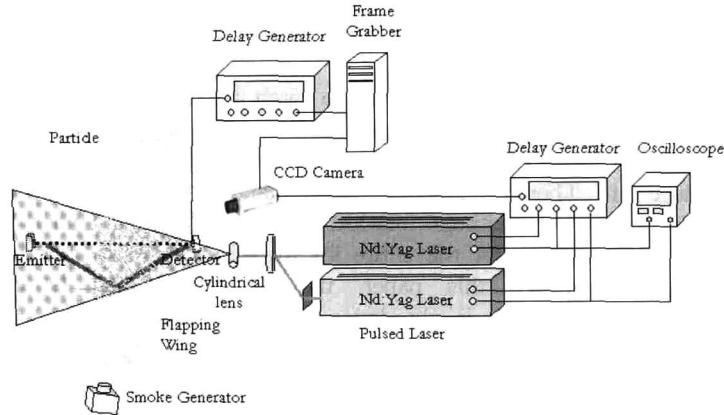
IV. Experimental Set Up

Fig. 3. PIV system set up for cross correlation by two lasers

V. Force Distribution During Flapping Motion

A. Flapping Mechanism and Various Wings

The flapping mechanism was adapted from a Cybird P2 remote control ornithopter model. The flapping mechanism is powered by a DC power supply.

Fig. 4 shows the operating angle of the flapping wing at a flapping frequency of 4 Hz using the 15 cm x 10 cm flat wing. Fig. 5 and Table 1 show the various wings, which were used in the experiment. The transparent plastic with 0.1mm thickness was used for wing surface, and carbon fiber sticks were used for the frame. The flapping mechanism was set at various flapping frequencies using a high precision strobe. The operating angle of the flapping wing mechanism is a weak function of the wing length, the wing material and the flapping
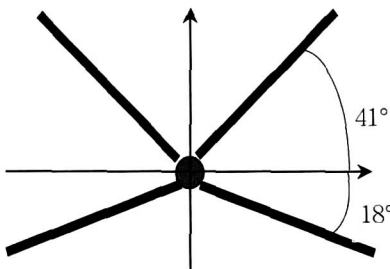

Fig. 4. The operating angle of the flapping mechanism at a flapping frequency of 4Hz
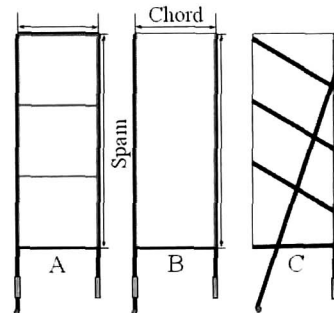

Fig. 5. Various wing shapes tested

Table 1. Various wings used in the experiment

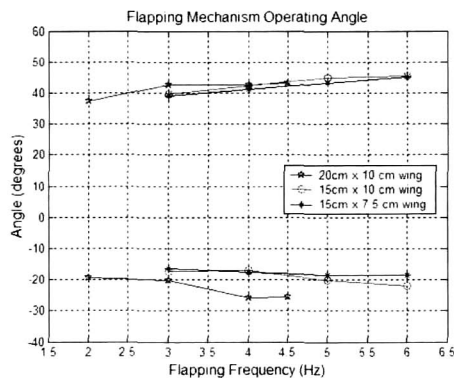| Wing#	Semi–Span(cm)	Chord(cm)	Aspect Ratio	Type	Flat or Cambered
1	20	10	4	A	Flat
2	15	10	3	C	Flat
3	15	7.5	4	C	Flat
4	15.5	7.5	4.1	B	Flat
5	5.5	7.5	1.5	B	Flat
6	15.5	7.5	4.1	B	Cambered*
* Curved 22 degrees at 5 cm from the end of the wing					

Fig. 6. The operating angles of the flapping mechanism as a function of flapping frequency
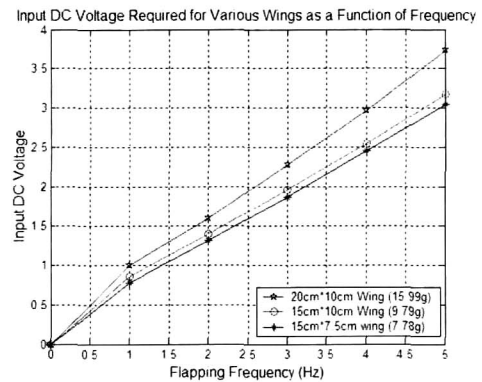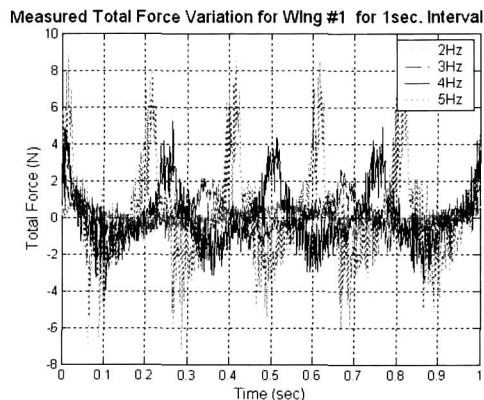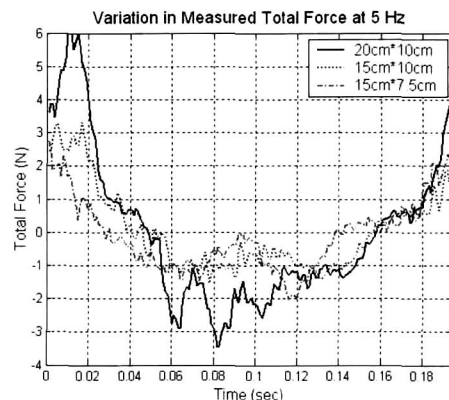

Fig. 7. The input D.C. Voltage required to flap the various wings as a function of flapping frequency

(a) The lift force variation as a function of time for different flapping frequencies for the 20cm*10cm wing for a 1 second time interval

(b) The total lift force variation of various wings at a flapping frequency of 5 Hz

Fig. 8. Force variation of flapping wing

frequency. As an example, Fig. 6 shows the flapping wing operating angle as a function of the flapping frequency. As the flapping frequency increases, the operating angles of the flapping wings also increase. The input D.C voltage required to flap these wings is shown in Fig. 7. The input D.C. voltage is directly proportional to the flapping frequency. The input D.C. voltage also depends upon the mass and area of the wing.

Fig. 8(a) presents the variation in lift force with flapping frequency for a 1 second time interval. A higher flapping frequency resulted in a larger lift force. Fig. 8(b) shows the total lift force variation with time for 3 of the wings tested. This total force will subsequently be divided up into the force due to the combination of the mass of wing and it's velocity as a function of time and the aerodynamic force due to the flapping motion. Since the inertial force is a direct function of the mass of the wing, the total force is also related to the mass of the wing. In addition, it can be observed that the aerodynamic force is a function of the area and AR of the wing.

B. Inertial Force

Inertial Forces represent the acceleration force on the mass of the wing as well as the added mass of the fluid around the wing. Some estimates of overall wing inertia suggest that inertial forces are generally higher than aerodynamic forces[13]. A vacuum container and a brass rod substituting for the uniform wing can be used to measure the inertial forces of the flapping mechanism. An accelerometer can also measure the force due to the mass of wing at the mechanism's body center[14]. The inertial force produced by wing motion cannot accelerate the mechanism's center of mass. Sane used the blade element method to estimate the inertial forces[15]. In our case, a high frame rate camera (FASTCAM   Ultima ADX 1000 frame/sec) is used to take the images of the flapping mechanism/wing using a fixed frame rate (constant time interval between images). Then, angular velocity and angular acceleration can be obtained from these images. The forces in the x and y direction of the flapping mechanism are calculated using angular velocity and angular acceleration(Eq. 1).

$$(a)\, \omega = \frac{\Delta \theta}{\Delta t}, \quad (b)\, \alpha = \frac{\Delta \omega}{\Delta t}, \quad (c)\; V_T = r\omega, \quad (d)\; a_T = r\alpha, \quad (e)\; F = ma \qquad (1)$$

where V_t and a_T are the tangential velocity and the tangential acceleration of the wings. Approximate values are required to generate the inertial force distribution from a set of experimentally determined discrete points using a polynomial in which the least squares interpolant (Eq. 2) has a minimum value from a 2nd to a 9th order polynomial. Fig. 9(a)
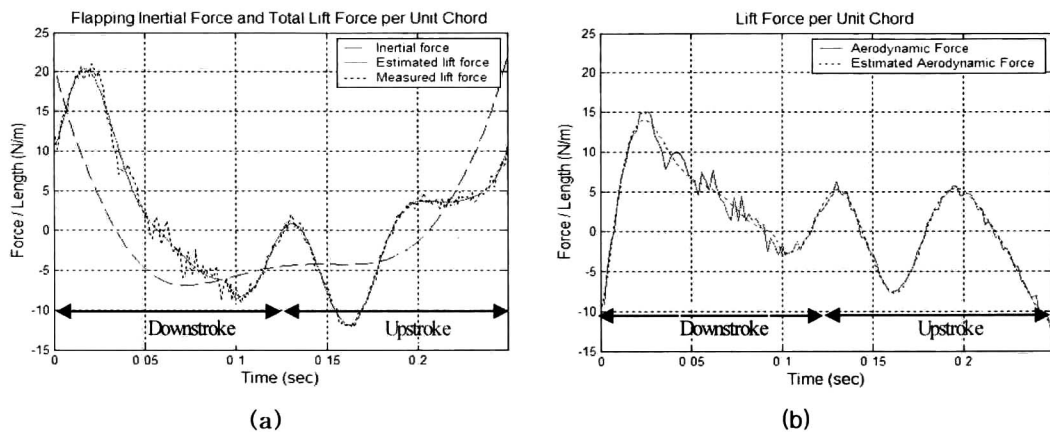

Fig. 9. The force variation of flapping wing during one entire cycle with wing #2 at 4 Hz flapping frequency

(a) The total force variation as measured by the force transducer (black dotted line), the polynomial curve fit approximation of the total force variation (red solid line), and the inertial force variation (blue dashed line) through one cycle from the beginning of the downstroke to the end of upstroke. (b) The polynomial curve fit approximation of the aerodynamic contribution to the lift force (dotted blue line) and the lift force (red solid line) resulting from the aerodynamic force.

shows the total lift force variation, the estimated total lift force variation and the inertial force variation throughout the entire cycle from the beginning of the downstroke to the end of upstroke. Fig. 9(b) shows the resulting lift force contribution of the aerodynamic force in which the inertial force is subtracted from the total lift force measured by the force transducer. The trends for temporal variation in total aerodynamic lift force and measured total lift force have nearly identical shape.

$$E = \sum_{i=1}^{n} \left[y_i - \hat{y} \right]^2 \qquad (2)$$

C. The Sub Phases of Flapping Motion

In referring to fig. 10, the full cycle of the flapping motion will be divided into 6 sub phases for the purposes of evaluation of the transient forces using the DPIV results. The justification behind the observations regarding the sense of the lift forces generated during each phase and their magnitude will be treated exhaustively in Section VI. In order to simplify the explanation later, the 6 sub phases will be introduced first.

1) The start of the downstroke: This phase begins from the starting point of the downstroke to the acceleration of the wing. Hence, acceleration is maximized in the downward direction. At the beginning of the downstroke, the inertial lift force is the greatest (+). Initially,
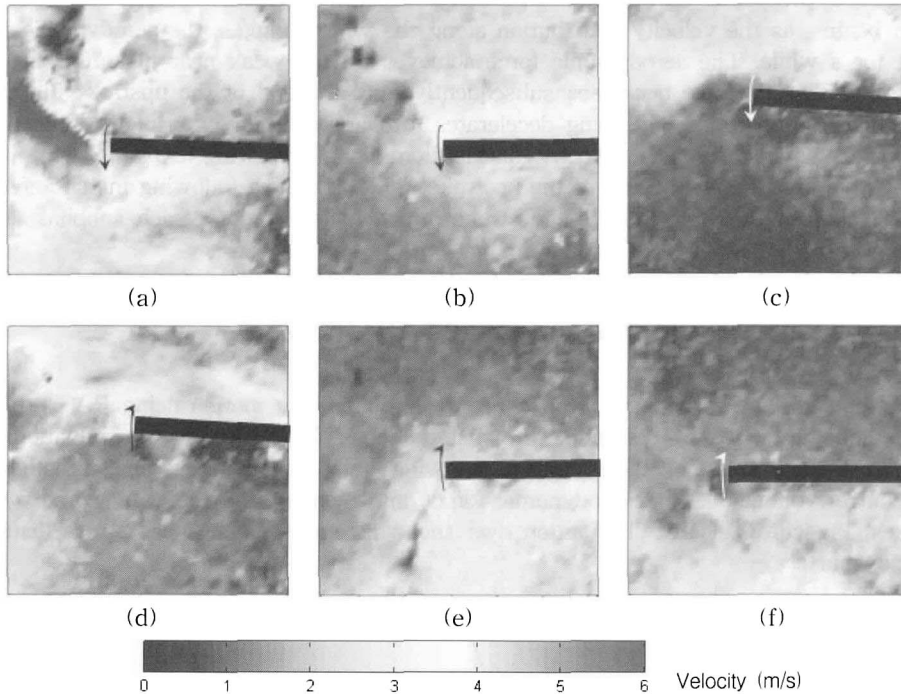

(a)   (b)   (c)

(d)   (e)   (f)

0   1   2   3   4   5   6   Velocity (m/s)

Fig. 10. PIV images at different locations in the flapping arc during the flapping motion with wing #2 at 4 Hz flapping frequency. The flap angle of each position is as follows: (a) +39° (b) 1° (c) 16° (d) 17° (e) 1° (f) +38°

(a) The initial stage of the stroke to downward – It is shown that there is a spanwise velocity difference between the upper and lower surfaces of the wing. The wing normally generates a negative lift force at this location in the flap arc. (b) During the downstroke, the wing can generate a positive lift force due to the velocity distribution across the lower and upper surfaces. (c), (d) Near the end of the downstroke and the start of the upstroke. The wing usually generates positive lift force. (e), (f) The stages including the upstroke. The flapping wing usually generates a negative lift force.

the resulting aerodynamic force is reflected in negative lift force, most likely because the spanwise velocity over the bottom surface of the flapping wing is greater than the velocity over the top surface(Fig. 10(a)).

2) The downstroke phase: The wing moves downward along the flap arc. The wing is accelerated while moving downward. It is also decelerated as it approaches the end of the downstroke. In the middle of the downstroke, the acceleration is zero. The inertial force decreases continuously until the point where the deceleration starts near the end of the downstroke. The aerodynamic force peaks at a specific point in the downstroke. The peak point is affected by the velocity distribution along the wing and the vortex effect(Fig. 10(b)).

3) The end of the downstroke: The wing is decelerated to change the direction of the flapping wing from downward to upward. As the deceleration progresses, the inertial lift force increases slightly. The aerodynamic force experiences a small peak almost at the end of the downstroke due to the velocity distribution along the wingspan(Fig. 10(c)).

4) The start of the upstroke: The wing is accelerated upward to begin moving upward. The acceleration is then maximized in the upward direction. The inertial force increases continuously until the end of the upstroke. The aerodynamic force creates a positive lift force, in spite of the upstroke, due to the velocity distribution across the wing(Fig. 10(d)).

5) The upstroke phase: The wing moves upward through the flapping arc. The wing is accelerated while moving upward. It is also decelerated as the wing approaches near the end of the upstroke. In the middle of the upstroke, the acceleration is zero. The aerodynamic force is usually negative lift force during the unfeathered upstroke. However, near the point that deceleration begins, as the velocity distribution along the wing changes, the aerodynamic force is positive lift for a while. The aerodynamic force achieves a small peak near just after the middle of the upstroke. The lift force decreases subsequently until the end of the upstroke(Fig. 10(e)).

6) The end of the upstroke: The wing decelerates to change the direction of the flapping wing from upward to downward. The velocity distribution along the wing explains why it could generate negative lift force at the end of the upstroke(Fig. 10(f)). The following instantaneous PIV images were taken of the wingtip with the stroke direction indicated for each subphase.

VI. Analysis of the Forces Resulting From Flow in the Spanwise Direction

To evaluate the force variation of an entire cycle of flapping motion using PIV results, two common methods are used to determine the instantaneous force; the direct evaluation of the pressure and the shear stress on the surface of the wing[16] and a momentum based method using a moving control volume[17,18]. The aerodynamic forces and moments on the wing come from two basic sources; Pressure/Velocity distribution over the wing surface and shear stress distribution over the body surface.
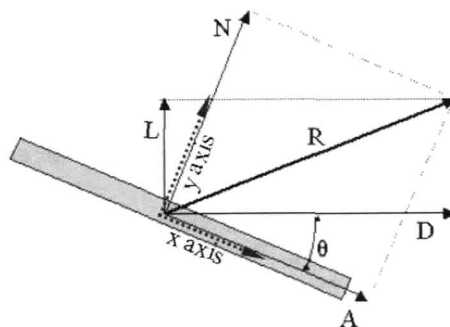

Fig. 11. Applied force along the wing

As seen in Fig. 11, normal force (N) is the component of the resultant force (R) perpendicular to the wing. Axial force (A) is the component of the resultant force (R) parallel to the wing. The normal and axial forces acting on the wing surface are

$$N = -\int P_u dS_u + \int P_l dS_l$$

(3)

$$A = \int \tau_u dS_u + \int \tau_l dS_l$$

(4)

As a meaningful definition for a velocity that scales the problem has not yet been established, Lift (L) is defined as the component of the resultant force (R) and the component of force opposite to gravity. Drag (D) is also defined as the component of the force perpendicular to the lift force (L).

The pressure and the shear stress method is formulated as follows(Eq. 5, 6).

$$L = \int \left[-P_u \cos\theta - \tau_u \sin\theta \right] dS_u + \int \left[P_l \cos\theta - \tau_l \sin\theta \right] dS_l$$

(5)

$$D = \int \left[-P_u \sin\theta + \tau_u \cos\theta \right] dS_u + \int \left[P_l \sin\theta + \tau_l \cos\theta \right] dS_l$$

(6)

where, P_u and P_l are the pressure on the upper and lower surfaces and τ_u and τ_l are the shear stresses along the wing at the upper and lower surface. θ is the angle of the flapping wing along the flap arc. The pressure distribution along the wing surface can also obtained by integrating the momentum equations[21] (Eq. 7, 8) along the x and y directions or from the pressure Poisson equation[19] (Eq. 9) while making fewer assumptions.

$$\frac{\partial u}{\partial t} + u\frac{\partial u}{\partial x} + v\frac{\partial u}{\partial y} = -\frac{1}{\rho}\frac{\partial p}{\partial x} + \frac{\mu}{\rho}\left[\frac{\partial^2 u}{\partial x^2} + \frac{\partial^2 u}{\partial y^2}\right]$$

(7)

$$\frac{\partial v}{\partial t} + u\frac{\partial v}{\partial x} + v\frac{\partial v}{\partial y} = -\frac{1}{\rho}\frac{\partial p}{\partial y} + \frac{\mu}{\rho}\left[\frac{\partial^2 v}{\partial x^2} + \frac{\partial^2 v}{\partial y^2}\right]$$

(8)

$$\nabla^2 p = -\rho \nabla \cdot (u \cdot \nabla u) = -\rho\left[\left(\frac{\partial u}{\partial x}\right)^2 + \left(\frac{\partial v}{\partial y}\right)^2 + 2\frac{\partial u}{\partial y}\frac{\partial v}{\partial x}\right]$$

(9)

where, u and v are velocities in x and y direction. The x and y axes are defined as the parallel and perpendicular axes of the flat wing surface (Fig. 11). The problem will be treated with increasing complexity later in the paper, but to begin with, several simplifying assumptions will be made. In the most simplified approach, the following assumptions are made:

the flow is steady $\left(\frac{\partial u}{\partial t}, \frac{\partial v}{\partial t} = 0\right)$, taken as a snapshot in time, incompressible (ρ = constant), irrotational ($\nabla \times V = 0$) flow along a streamline. Following these assumptions for this simplified case, Bernoulli's equation can be used to obtain the pressure distribution along the wing.

$$p = p_r - \frac{1}{2}\rho V^2$$

(10)

A momentum based method using a moving control volume can also be applied to determine the force generated by the flapping wing using PIV velocity data. The velocities of the control volumes in the x and y direction (U_i, V_i) are determined from the results of analysis of images taken with a high frame rate camera (FASTCAM - Ultima ADX - 1000 fps). PIV results provide the velocity data along the wing during the flapping motion (Fig. 13).
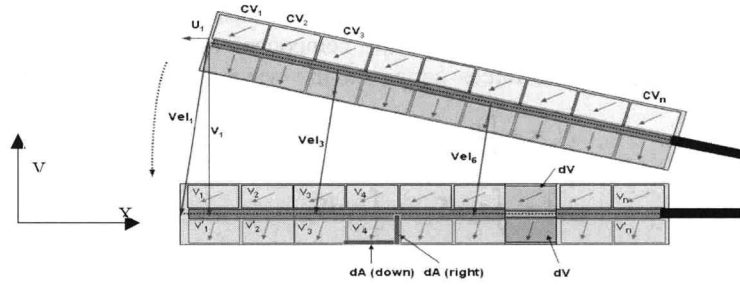
Fig. 12. Control volume to calculate the instantaneous force around the flapping wing
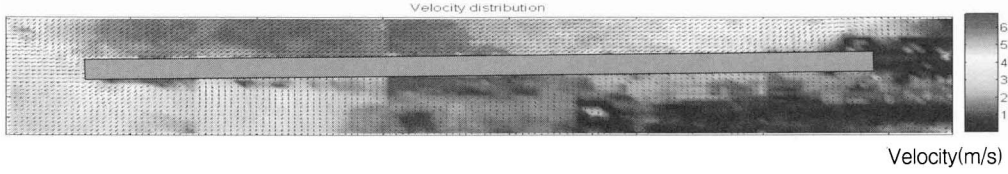

Velocity(m/s)

Fig. 13. A composite of instantaneous PIV images taken along the entire semi-span of the wing with wing #1 at 4 Hz flapping frequency

If the flapping wing and the area immediately surrounding it is defined as the control volume, the wing can be divided into several smaller control volumes. Each smaller control volume includes a velocity vector over the wing and under the wing (Fig. 12). As a result, the momentum equation for accelerating control volumes is applied to the total control volume that includes wing and velocity vectors along the wing.

For an inertial control volume, the appropriate formulation of Newton's second law is given by:

$$\vec{F} = \frac{\partial}{\partial t} \int_{cv} \vec{V}_{XYZ}\, \rho_{cv}\, dV + \int_{cs} \vec{V}_{XYZ}\, \rho_{cs} \vec{V}_{xyz} \cdot d\vec{A} \tag{11}$$

From Eq (11),

$$\vec{F} = \vec{F}_{Surface} + \vec{F}_{Body} + \vec{F}_{Resultant} \tag{12}$$

where, surface force ($\vec{F}_{Surface}$) is the sum of pressure and shear force ($\vec{F}_{Surface} = \vec{F}_{Pressure} + \vec{F}_{Shear}$). $\vec{F}_{Body}$ is the body force and $\vec{F}_{Resultant}$ is the resultant force which exerts equal and opposite pressure and shear force distribution on the flow from the body by Newton's third law.

Therefore, the Eq (11) becomes

$$\vec{F}_{Pressure} + \vec{F}_{Shear} + \vec{F}_{Body} + \vec{F}_{Resultant} = \frac{\partial}{\partial t} \int_{cv} \vec{V}_{XYZ}\, \rho_{cv}\, dV + \int_{cs} \vec{V}_{XYZ}\, \rho_{cs} \vec{V}_{xyz} \cdot d\vec{A} \tag{13}$$

If flow is inviscid and $\vec{F}_{Body} \ll \vec{F}_{Pressure}$ because the control volume is selected around the air, then, the shear forces ($\vec{F}_{Shear}$) and body forces ($\vec{F}_{Body}$) have nominal values and can be omitted. Therefore, Eq (13) becomes

$$\vec{F}_{Resultant} \approx -\vec{F}_{Pressure} + \frac{\partial}{\partial t} \int_{cv} \vec{V}_{XYZ} \rho_{cv}\, dV + \int_{cs} \vec{V}_{XYZ} \rho_{cs} \vec{V}_{xyz} \cdot d\vec{A} \tag{14}$$

Resultant force (lift or drag) is equal to the sum of the pressure force (or normal force (N)), the time rate of change of the momentum inside the control volume selection and the net rate of momentum flux out through the control surface.

The velocity with respect to the inertial frame (XYZ) and the reference frame (xyz) is related by the relative motion equation.

$$\vec{V}_{xyz} = \vec{V}_{XYZ} - \vec{V}_{rf} \tag{15}$$

where, $\vec{V}_{rf}$ is the velocity of the control volume reference frame.

Then, the sum of the time rate of change of the momentum inside the control volume selection and the net rate of momentum flux out through the control surface in the y direction is written as follows:

$$\frac{\partial}{\partial t}\int_{cv}\vec{V}_{XYZ}\rho_{cv}d\mathcal{V} + \int_{cs}\vec{V}_{XYZ}\rho_{cs}\vec{V}_{xyz}\cdot d\vec{A} = \sum_{i=1}^{n}\begin{bmatrix} \frac{d}{dt}\int_{cv(Upper)}\rho v_{yi}d\mathcal{V} + \int_{cs(Upper\_LH)}v_{yi}\rho[(v_{xi}-U_{i})\cos\alpha-(v_{yi}-V_{i})\sin\alpha]\cdot nd\vec{A} \\ + \int_{cs(Upper\_RH)}v_{yi}\rho[(v_{x(i+1)}-U_{i})\cos\alpha-(v_{y(i+1)}-V_{i})\sin\alpha]\cdot nd\vec{A} \\ + \int_{cs(Upper\_Top)}v_{yi}\rho[(v_{xi}-U_{i})\sin\alpha+(v_{yi}-V_{i})\cos\alpha]\cdot nd\vec{A} \\ + \frac{d}{dt}\int_{cv(Lower)}\rho v'_{yi}d\mathcal{V} + \int_{cs(Lower\_LH)}v'_{yi}\rho[(v'_{xi}-U_{i})\cos\alpha-(v'_{yi}-V_{i})\sin\alpha]\cdot nd\vec{A} \\ + \int_{cs(Lower\_RH)}v'_{yi}\rho[(v'_{x(i+1)}-U_{i})\cos\alpha-(v'_{y(i+1)}-V_{i})\sin\alpha]\cdot nd\vec{A} \\ + \int_{cs(Lower\_Bottom)}v'_{yi}\rho[(v'_{xi}-U_{i})\sin\alpha+(v'_{yi}-V_{i})\cos\alpha]\cdot nd\vec{A} \end{bmatrix} \tag{16}$$

where, V_i and U_i is the y and x components of the control volume velocity, and v'_{xi} (v_{yi} and v'_{yi}) are the x components (y components) of the air flow velocity (v_i and v'_i in fig. 12) over the upper surface and lower surface of the wing. α is the angle of flapping wing in flapping arc. The force in the x direction of the flapping wing is obtained using the same method.

From the Conservation of Mass,

$$\frac{\partial}{\partial t}\int_{cv}\rho d\mathcal{V} + \int_{cs}\rho\vec{V}_{xyz}\cdot d\vec{A} = 0 \tag{17}$$

When density (ρ) and volume ($\mathcal{V}$) are constant, the conservation of mass for incompressible flow through a fixed control volume becomes

$$\int_{cs}\rho\vec{V}_{xyz}\cdot d\vec{A} = 0 \tag{18}$$

The Conservation of Mass is satisfied in 3 dimensions (spanwise and chordwise plane). However, if we assume steady state in the case for satisfying the Conservation of Mass, the time rate of change of the momentum inside the control volume ($\frac{\partial}{\partial t}\int_{cv}\vec{V}_{XYZ}\rho_{cv}d\mathcal{V}$) has no value ("zero" value), and the net rate of momentum flux out through the control surface ($\int_{cs}\vec{V}_{XYZ}\rho_{cs}\vec{V}_{xyz}\cdot d\vec{A}$) also approaches zero. Therefore, the net lift force in 3 dimensions for steady flow is equal to the pressure/shear force for our defined control volume.

A. Lift Force Distribution Along the Entire Wing from the Wing Root to the Wingtip

As seen in fig. 14, there are strong flow velocities in the spanwise plane over the wing at the middle of the downstroke. The y component velocities over the lower and upper surface of the wing are almost proportional to the tangential velocity of the wing (Fig. 14(b)). However, spanwise velocities (x component) over the upper surface of the wing are greater than spanwise velocities over the lower surface of the wing (Fig. 14(a)). Fig. 14(c) shows the calculated force distribution on the wing determined by substituting PIV data (speed ($\sqrt{u^2 + v^2}$)) into the above methods for pressure/shear, along the entire semi span at a fixed point in the flapping arc. The lift force distribution directly shows the contribution of flow in the spanwise plane towards the generation of lift.
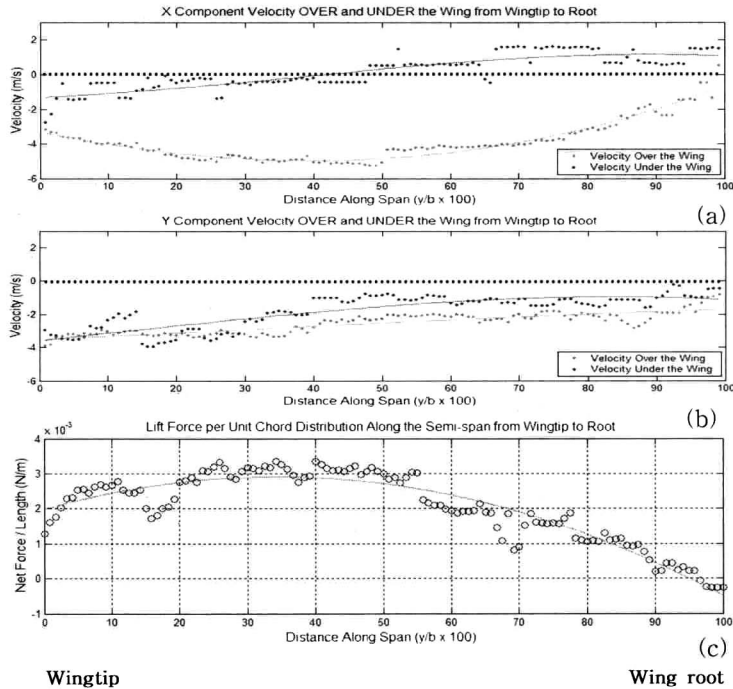
**Fig. 14. Velocity and lift force distribution along the wingwith wing #1
at 4 Hz flapping frequency**

(a) The x component (spanwise flow) velocity distribution along the entire semi span of the wing over and under the wing. (b) The y component velocity distribution along the entire semi span of the wing over and under the wing. (c) Lift force distribution from the contribution of the pressure and shear force distribution in the spanwise plane (2 dimensions in spanwise plane)

B. Flat Plate and Spanwise Cambered Wings

Most aircraft and bird wings are cambered in chord to generate more lift at lower angles of attack. The effects of cambering wings in the chordwise sense are well documented. However, the effects of cambering wings in the spanwise direction have not been quantified as yet. Spanwise camber is observed in the flight of most birds, bats and insects. Insects have been found to have up to 4% camber in span[20]. Dudley[21], Pennycuick[22]., Combes and Daniel[23,24] have discussed the advantages of having wings curved in span. Ennos[25] showed that the presence of spanwise bending due to the inertia of flapping wings could produce at least twice as much aerodynamic force than in rigid wings.

In this section, the experiments performed to compare the aerodynamic lift force generated by pure flapping of a spanwise cambered wing and a flat plate wing will be discussed. The cambered and flat plate wings have the same mass, material, area, and aspect ratio (Wing # 4 and # 6 in Table 1). The cambered wing was only cambered in the spanwise direction. Velocity data was acquired in the last 1 cm of the tip of the flapping wing to quantitatively compare the differences in the cambered and flat plate wings at the tip. Due to the reflection of the laser off of the wing surface, the velocity vectors were obtained at a height of 4 mm from the wing surface.

A representative set of results can be seen in Fig. 15. The difference in speed (scalar value) distributions across the upper and lower surfaces between the downstroke and upstroke can readily be observed with the downstroke experiencing a much greater difference. In addition, when comparing the cambered and uncambered wing cases in the downstroke, clearly

(a)   (b)

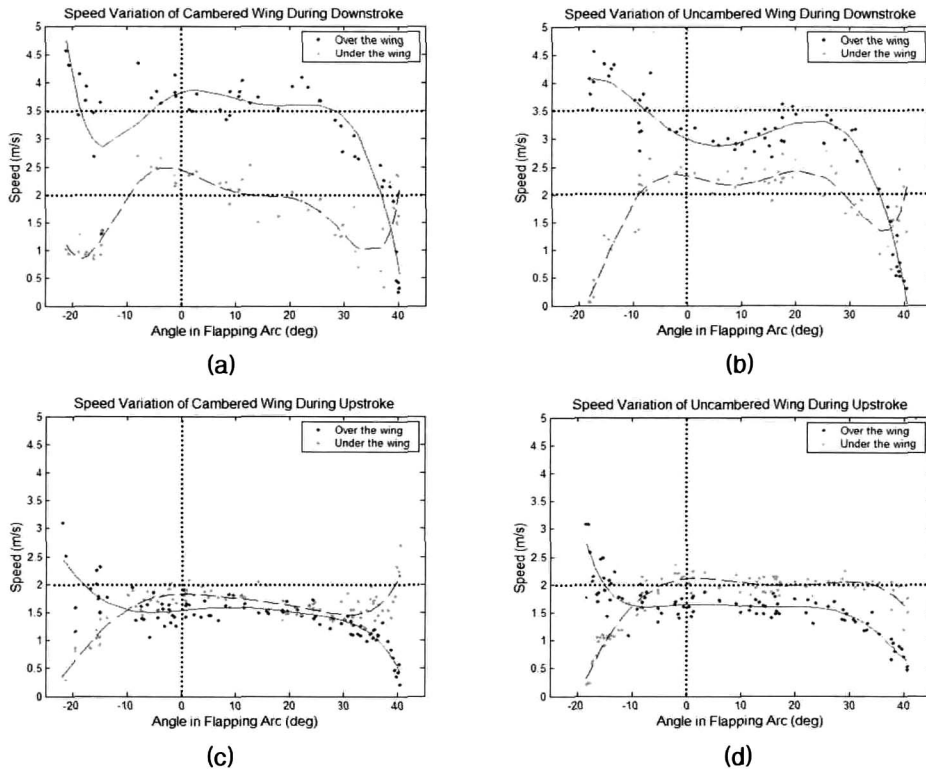(c)   (d)

Fig. 15. The speed variation of the air over the upper and the lower surfaces of the wing for the cambered and flat plate wings in pure flapping hover

(a) The (spanwise) speed variation across the uncambered wing during the downstroke (b) The (spanwise) speed variation across the cambered wing during the downstroke (c) The (spanwise) speed variation across the uncambered wing during the upstroke (d) The (spanwise) speed variation across the cambered wing during the upstroke The red and blue points are the speed variation which was selected from the PIV results over the top and bottom surface of the wing during the downstroke and upstroke. The red solid line and blue dashed line are the approximated speed variation over the top and bottom surface of the wing using a 6th order polynomial. Wing # 4 and # 6 were used at a 4 Hz flapping frequency. The velocity data were acquired in the last 1 cm (6.5% semi span) of the flapping wing.

a greater speed difference from upper to lower surface exists for the cambered wing case. Applying the simplified model (Bernoulli's equation) using speed ($\sqrt{v_x^2 + v_y^2}$), it follows that for the set of points being considered; force is generated locally in the upward direction (lift) during the downstroke. Accordingly, the flapping wing unfeathered during the upstroke will generate a negative lift force, albeit much smaller in magnitude.

Curiously, although the cambered wing generates higher speeds over the upper wing surfaces during the downstroke than the flat wing (Figs. 15(a) and (b)), the cambered wing generates lower speeds over the lower wing surfaces than the flat wing until near the zero flapping angle in the flap arc. During the upstroke, these effects are reversed, again having much lower magnitude. As can be seen in Fig. 16, the upper to lower surface spanwise speed difference is directly temporally related to the generation of lift force by the mechanism. It is therefore expected that the cambered wing and the flat wing will have a different variation in aerodynamic force during the flapping cycle. Fig. 16 shows the calculated lift force variation through the flapping cycle resulting from the normal force (N) approximated using Bernoulli's equation and the axial force (A) approximated using the shear stress during the full flapping cycle. The cambered wing generates more positive lift force than the flat wing during
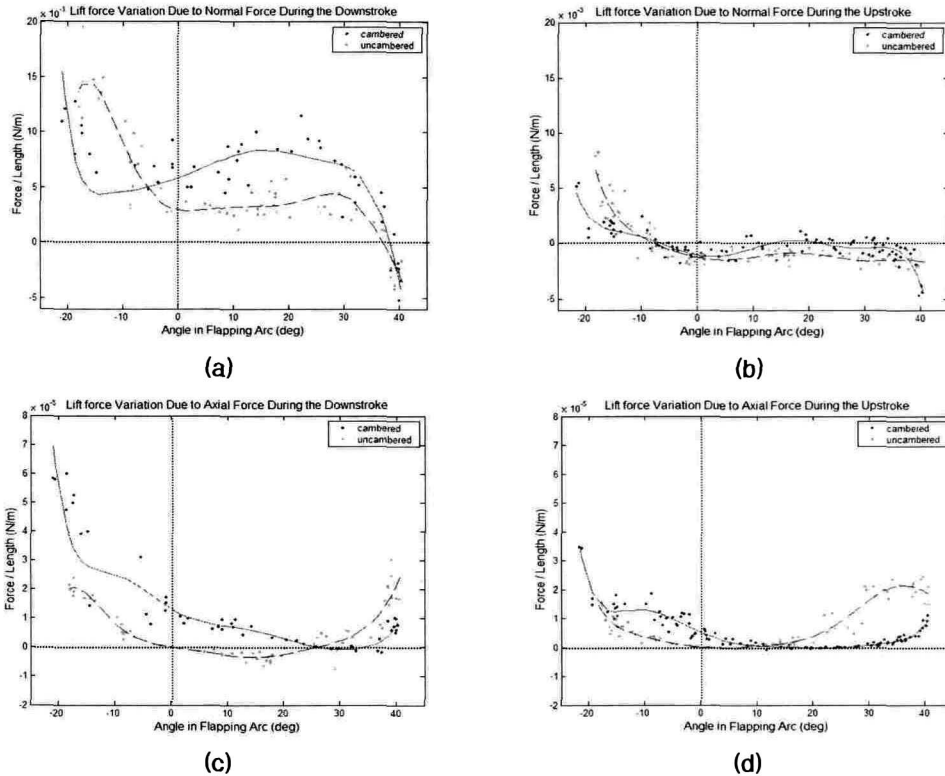
(a)

(b)

(c)

(d)

Fig. 16. The lift force variation due to the normal and axial forces in cambered and flat wings calculated from PIV velocity vectors (Wing # 4 and # 6 at 4 Hz flapping frequency)

(a) The lift force variation due to normal force in cambered and flat wings during the downstroke (b) The lift force variation due to normal force in cambered and flat wings during the upstroke (c) The lift force variation due to axial force in cambered and flat wings during the downstroke (d) The lift force variation due to axial force in cambered and flat wings during the upstroke. The blue and red dots indicate the variation in force calculated from the PIV results for the uncambered and cambered wings. The blue dashed and red solid lines represent the approximate force variation for the uncambered and cambered wings using a 6th degree polynomial, The lift force variation have discontinuities at the end of down and upstroke, because data which are used to calculate the force has discontinuities near the end of down and upstroke. Velocity data also include error components because of not average realization but single PIV realization.

downstroke and upstroke as seen in Figs. 16(a) and (b). From observing the axial force variation, it can be inferred that the airflow runs parallel to the wing surface at the beginning and end of each stroke. The axial force of the flat wing is slightly greater than that of the cambered wing at the beginning of the downstroke and the end of the upstroke. The axial force of the cambered wing is in fact greater than that of the flat wing at the end of the downstroke and the beginning of the upstroke. However, the magnitude of the axial force is substantially smaller than the magnitude of normal force.

From the results for the lift force variation due to the normal force (N) and axial force (A), the flapping motion generates a negative total lift force at the beginning of the downstroke. The lift force then increases until it peaks. The lift force then decreases until near the end of the downstroke. Both the cambered and flat wings produce another peak force almost at the end of the downstroke. During the downstroke, the cambered wing produces a greater lift force than the flat wing at the middle of the downstroke. Both wings generate another local peak lift force at the beginning of the upstroke. There is no notable difference in the two wings in the middle of the upstroke. The cambered wing does however generate a
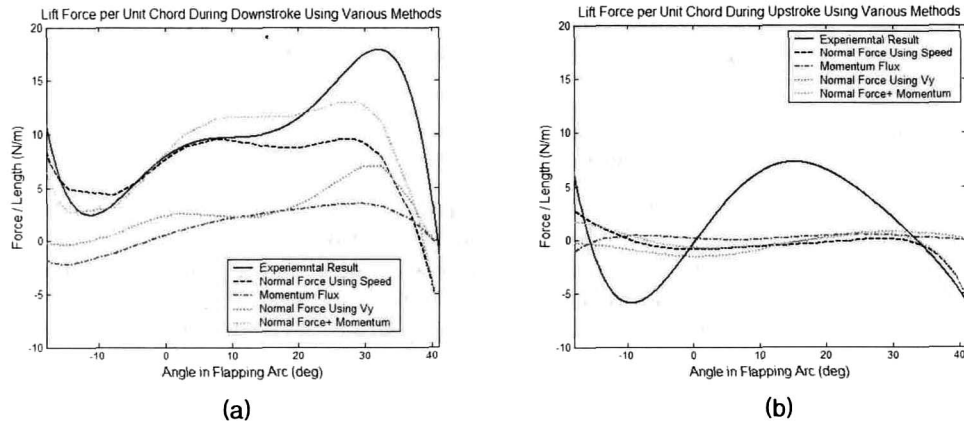
(a)   (b)

Fig. 17. Lift force variation due to the aerodynamic force obtained using the high-speed camera and force transducer, due to normal force (N) calculated with speed ($\sqrt{u^2 + v^2}$) and perpendicular velocity (v), and due to momentum flux during the downstroke and the upstroke

(a) Lift force variation during the downstroke (b) Lift force variation during the upstroke. Velocity data for calculating the force were acquired in the last 1 cm of the tip of the flapping wing and the interrogation area for one velocity vector is 0.14 cm×0.14 cm. The force variation due to the aerodynamic force obtained using the high-speed camera and force transducer is measured from a wing with dimensions of 15.5 cm×10 cm. Therefore, the force calculated using normal force and momentum flux is multiplied by 120 to qualitatively compare the differences and similarities in the curves

slightly lower magnitude negative lift force than the flat wing. Near the end of the upstroke, the flat and cambered wings produce a negative lift force once again. When taken together, the results for this method confirm that the lift force produced by the cambered wing during both the downstroke and the upstroke generate greater lift force than the flat (uncambered) wing. The total lift force determined from the normal force/shear force for the cambered wing during the downstroke is greater than the total lift force due to normal force/shear force of the uncambered wing (Fig. 16). In observing Fig. 16, the cambered wing can generate more lift until almost the middle of the downstroke. After the middle of the downstroke, flat wing generates more lift than the cambered wing. As seen in Fig. 17, the results in Fig. 16 agree well with the trends in lift force variation seen previously (in Fig. 9(b)) due to the aerodynamic force obtained using the high speed camera and force transducer, especially during downstroke. However, PIV results were obtained in 3 dimensional plane, not 2 dimensional plane, and they were used to calculate the force assuming 2 dimensions. Therefore, the magnitude of lift force due to the aerodynamic force obtained using force transducer does not agree well with lift force due to normal force with speed ($\sqrt{u^2 + v^2}$). The net lift force variation calculated with normal force using speed ($\sqrt{u^2 + v^2}$) shows greater lift force than the net lift force variation calculated with normal force using v (perpendicular velocity to the wing) during the whole cycle. When taken together, the results confirm that the flow in spanwise plane contributes to the generation of lift force, especially during downstroke.

VIII. Conclusion

A flat plate flapping wing without forward relative velocity and without pitch change generates lift force. Even though the presence of spanwise fluid dynamic structures have previously been identified, no attempt has been made to quantify this lift force due to spanwise

flow. A method has been identified and presented to determine the aerodynamic forces due exclusively to flow in the spanwise direction from the flapping motion, using PIV results combined with two different methods:

1) The direct evaluation of the pressure and the shear stress on the surface of the wing.
2) A net rate of change of momentum flux using a moving control volume.

It has been shown that spanwise flow is responsible for the generation of lift during the flapping motion. The effect of cambering a flapping wing in span was shown to be advantageous to the creation of greater aerodynamic force. It follows that there is the *possibility* of a similar direct contribution of flow in the spanwise plane to the generation of lift in flapping animals. Regardless, exploitation of this effect should be investigated for use in an artificial flapping wing vehicle.

Reference

1 Birch J. M, Dickinson M. H, "Spanwise Flow And The Attachment Of The Leading-Edge Vortex On Insect Wings", Nature, Vol. 412, pp. 688 689, 2001.
2 Ellington, C. P., Van den Berg, C. and Willmott, A. P., "Leading Edge Vortices In Insect Flight", Nature, Vol. 384, pp. 626 – 630, 1996.
3 Taylor, G. S., Schnorbus, T., and Gursul, I. "An Investigation of Vortex Flows Over Low Sweep Delta Wings", AIAA-2003-4021.
4 Batchelor, G. K., "Axial Flow In Trailing Line Vortices", Journal of Fluid Mechanics. Vol.20. pp. 645 – 658, 1964.
5 Anderson, Elgin A., and Lawton, Todd A., "Correlation Between Vortex Strength And Axial Velocity In A Trailing Vortex", Journal of Aircraft, Vol. 40, No. 4, 2003.
6 Chow, Jim S., Zillac, Gregory G., Bradshaw, Peter, "Mean And Turbulence Measurements In The Near Field Of A Wingtip Vortex", AIAA Journal, Vol. 35, No. 10, October 1997.
7 Khorrami, M. R, "Computational Simulations Of A Three Dimensional High Lift Wing", AIAA-2002-2804.
8 Lian, Yongsheng and Shyy, Wei, "Numerical Simulations Of Membrane Wing Aerodynamics For Micro Air Vehicle Applications", Journal of Aircraft, Vol. 42, No. 4, July-August 2005.
9 Greenewalt, Crawford H., "Dimensional Relationships For Flying Animals", Smithsonian Institution, Washington D.C., 1962.
10 Azuma A., "The Biokinetics of Flying and Swimming", Springer-Verlag, Tokyo, 1992.
11 Lionel D. Alford, Jr, "A Definitive Macro-Aerodynamic Analysis Of Natural Flapping Flight", Ph. D Dissertation, University of Dayton, Department of Mechanical and Aerospace Engineering, 2006.
12 Birch, J. M., Dickson, W. B. and Dickinson, M. H., "Force Production And Flow Structure Of The Leading Edge Vortex On Flapping Wings At High And Low Reynolds Numbers", Journal of Experimental Biology, Vol. 207. pp.1063-1072, 2003.
13 Combes, S. A. and Daniel, T. L., "Into thin Air: Contributions Of Aerodynamic And Inertial-Elastic Forces To Wing Bending In The Hawkmoth Maduca Sexta", Journal of Experimental Biology, Vol. 206. pp.29993006, 2003.
14 Bilo, Dietrich, et al, "Measurement Of Linear Body Accelerations And Calculation Of The Instantaneous Aerodynamic Lift And Thrust In A Pigeon Flying In A Wind Tunnel", Biona-Report 3. Stuttgart, Gustav Fischer, 1985.
15 Sane, Sanjay P., and Dickinson, Michael H., "The Control Of Flight Force By A Flapping Wing: Lift And Drag Production", The Journal of Experimental Biology, Vol.204, pp. 26072626, 2001.
16 Maybury, Will J. and Lehmann, Fritz-Olaf, "The Fluid Dynamics Of Flight Control By Kinematic Phase Lag Variation Between Two Robotic Insect Wings", Journal of Experimental Biology, Vol. 207, pp. 4707-4726, 2004.
17 Noca F, Shiels D and Jeon D, "Measuring Instantaneous Fluid Dynamic Forces On Bodies, Using Only Velocity Fields And Their Derivatives", Journal of Fluids and Structures, Vol. 11, 1997.
18 Unal, M.F., Lin, J. C, and Rockwell, D., "Force Prediction By PIV Imaging, A

Momentum-Based Approach", Journal of Fluids and Structures, Vol.11, 1997.

[19] Gurka, R., Liberzon, A., Hefetz, D., Rubinstein, D., and Shavit, U., "Computation Of Pressure Distribution Using PIV Velocity Data", Proc. 3rd Int. Workshop PIV (Santa Barbara), 1999.

[20] Combes, S. A., and Daniel, T. L., "Flexural Stiffness In Insect Wings II. Spatial Distribution And Dynamic Wing Bending", The Journal of Experimental Biology, Vol. 206, 2003.

[21] Dudley, R., "The Biomechanics Of Insect Flight: Form, Function, Evolution", Princeton University Press, Princeton, NJ, 2000.

[22] Pennycuick, C. J., "Animal Flight", The Institute of Biology's Studies in Biology, No. 33, 1972.

[23] Combes, S. A., "Wing Flexibility And Design For Animal Flight", Ph.D. thesis, University of Washington, 2002.

[24] Daniel, T.L. "Forward Flapping Flight From Flexible Fins", Canada Journal of Zoology, Vol. 66, pp. 630-638, 1987.

[25] Ennos, A. R., "Inertial And Aerodynamic Torques On The Wings Of Diptera In Flight", Journal of Experimental Biology, Vol.142, pp.87-95, 1989.